

The dynamical evolution of transiting planetary systems including a realistic collision prescription

Alexander J. Mustill¹★, Melvyn B. Davies¹, Anders Johansen¹

¹Lund Observatory, Department of Astronomy & Theoretical Physics, Lund University, Box 43, SE-221 00 Lund, Sweden

Accepted XXX. Received YYY; in original form ZZZ

ABSTRACT

Planet–planet collisions are a common outcome of instability in systems of transiting planets close to the star, as well as occurring during *in-situ* formation of such planets from embryos. Previous N -body studies of instability amongst transiting planets have assumed that collisions result in perfect merging. Here, we explore the effects of implementing a more realistic collision prescription on the outcomes of instability and *in-situ* formation at orbital radii of a few tenths of an au. There is a strong effect on the outcome of the growth of planetary embryos, so long as the debris thrown off in collisions is rapidly removed from the system (which happens by collisional processing to dust, and then removal by radiation forces) and embryos are small ($< 0.1 M_{\oplus}$). If this is the case, then systems form fewer detectable ($\geq 1 M_{\oplus}$) planets than systems evolved under the assumption of perfect merging in collisions. This provides some contribution to the “*Kepler* Dichotomy”: the observed over-abundance of single-planet systems. The effects of changing the collision prescription on unstable mature systems of super-Earths are less pronounced. Perfect mergers only account for a minority of collision outcomes in such systems, but most collisions resulting in mass loss are grazing impacts in which only a few per cent. of mass is lost. As a result, there is little impact on the final masses and multiplicities of the systems after instability when compared to systems evolved under the assumption that collisions always result in perfect merging.

Key words: planets and satellites: dynamical evolution and stability — planets and satellites: formation — circumstellar matter

1 INTRODUCTION

An important challenge in modelling the formation and long-term dynamical evolution of planetary systems is to adequately model planet–planet collisions. Particularly at the short orbital periods probed by transit observatories such as *Kepler*, when planets collide their impact velocity can significantly exceed their surface escape velocity. The ratio of orbital to escape velocity for known exoplanets with measured masses and radii is shown in Figure 1¹. We also mark this ratio for the Solar System planets, and what the ratio would be if those planets were located at 0.1 au. The ratio of Keplerian to escape velocity increases towards smaller planetary masses. Super-Earths or terrestrial planets within ~ 0.1 au have $v_{\text{Kep}}/v_{\text{esc}} \gtrsim 10$, comparable to the value for our Solar System’s Mercury.

The resulting high impact velocities between planets or planetary embryos means that collisions do not result in perfect merging of the parent planets. A high-velocity impact may be responsible for the anomalously large core of the planet Mercury itself, mantle material having been blown off in the impact (e.g., Benz et al. 1988,

2007). Amongst the population of extrasolar planets discovered by *Kepler*, it has been suggested that the effects of high-velocity collisions may be responsible for planets in the same system showing large density differences (e.g., Kepler-36; Quillen et al. 2013), and for contributing to the multiplicity distribution of close-in transiting planetary systems (e.g., Volk & Gladman 2015). Debris produced in such collisions may be responsible for unusually bright warm debris discs (e.g., Song et al. 2005; Melis et al. 2010; Theissen & West 2017).

However, many N -body integrators such as MERCURY (Chambers 1999) implement collisions between bodies as perfect inelastic mergers, with two planets combining into one with no loss of mass or momentum (but indeed a loss of energy). In contrast, high-velocity collisions between planets and planetary embryos in reality can result in significant amounts of mass loss. In this paper we explore the effects of adopting a collision prescription more realistic than perfect merging on the observable multiplicities of planetary systems. We compare the final multiplicities of unstable multi-planet systems evolved under the assumptions of perfect merging with those evolved with a more realistic collision prescription. We conduct three experiments. First we set up unstable systems of planets at small orbital radii ($a < 1$ au), and explore the effects of changing the collision prescription on the final multiplicities and masses of

★ E-mail: alex@astro.lu.se

¹ Data from <http://exoplanets.org/> (Han et al. 2014) on 2017-04-25.

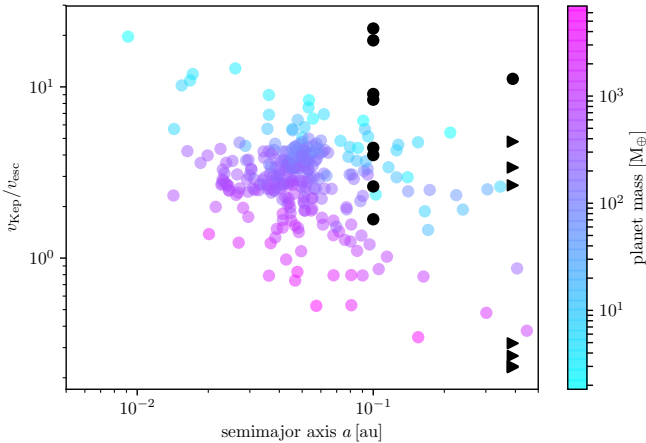


Figure 1. Ratio of Keplerian orbital velocity v_{Kep} to surface escape velocity v_{esc} for the 272 planets with known masses and radii listed in <http://exoplanets.org/>. The higher this ratio, the greater the chance that a planet–planet collision will be erosive. Symbols are coloured according to planet mass. The values for Solar System planets are marked as black symbols at the right of the plot (Mercury at its semimajor axis as a circle, the other planets as triangles). The black symbols at 0.1 au show the equivalent values for Solar System planets if they were orbiting at 0.1 au. Super-Earths orbiting at 0.1 au are in a more erosive regime than the Earth and Venus in our Solar System.

the planets. We then consider systems of transiting planets destabilised by outer planets experiencing planet–planet scattering or Kozai perturbations, as in our previous paper (Mustill et al. 2017). We show that the latter set has a much greater sensitivity to the collision prescription, largely owing to the greater eccentricities excited in these systems. Finally, we consider the effects of changing the collision algorithm on *in-situ* formation of rocky super-Earths.

The outcomes of high-velocity collisions between planets can be studied numerically, for example with Lagrangian smooth-particle hydrodynamics (SPH) or Eulerian adaptive mesh refinement (AMR) codes. Different algorithms or resolutions however often result in quantitatively different outcomes, even in so fundamental a property as the mass of the largest remnant after the collision (Genda et al. 2015; Liu et al. 2015; Reinhardt & Stadel 2017). Nevertheless, the qualitative nature of collision outcomes is understood, with low collision velocities (relative to the mutual escape velocity) leading to perfect merging, higher velocities leading to some mass loss (which may result in growth or erosion of the largest body), and very high velocities resulting in “supercatastrophic disruption” where $< 10\%$ of the original mass remains bound. Analytical scaling laws determining the boundaries between the different regimes and the outcomes in terms of remnant masses have been developed (Benz & Asphaug 1999; Genda et al. 2012; Leinhardt & Stewart 2012; Movshovitz et al. 2016). These analytical laws provide an acceptable means to compute collision outcomes, particularly given the lack of agreement or convergence in some hydrodynamical studies (e.g., Genda et al. 2015; Liu et al. 2015; Reinhardt & Stadel 2017). They also allow the outcome to be computed near-instantaneously, rather than requiring expensive hydrodynamical simulations to be conducted for each set of collision parameters. They are therefore ideally suited for incorporation into the N -body integrators used to study planet formation and stability, and several studies have now moved away from the perfect merging collision model to better

model planet formation in the terrestrial planet region at ~ 1 au (Chambers 2013; Carter et al. 2015; Leinhardt et al. 2015; Chambers 2016; Quintana et al. 2016) or interior (Wallace, Tremaine & Chambers 2017).

In this paper we adapt the collision model presented by Leinhardt & Stewart (2012), henceforth LS12, incorporate it into the MERCURY integrator (Chambers 1999), and study the effects of this on unstable close-in planetary systems detectable in transit at a few tenths of an au. We briefly introduce the expected collision environment for transiting planetary systems in Section 2. We describe the collision model in Section 3. We then describe the impacts of changing the collision model on systems purely composed of close-in planets in Section 4, and then on systems of close-in planets destabilised by outer planets in Section 5. We then examine the effects on *in situ* formation of rocky super-Earths in Section 6. We discuss and conclude in Section 7.

2 THE COLLISION ENVIRONMENT OF CLOSE-IN PLANETS

We begin by estimating the collision velocities that can be expected between transiting planets within a few tenths of an au. These must be compared to the planets’ surface escape velocities: the more the collision velocity exceeds the escape velocity, the more energy is available to unbind a fraction of the total mass, and the worse an approximation perfect merging is to the true collision outcome.

First consider one planet on a circular orbit at semimajor axis a_1 , with a second planet on a wider coplanar orbit of semimajor axis a_2 and pericentre $q_2 = a_1$, so that its orbit just touches that of the first planet and collisions can occur at pericentre. The orbital Keplerian velocity of the inner planet is

$$v_{\text{Kep},1} = \sqrt{\mathcal{G}M_{\star}/a_1}, \quad (1)$$

while the pericentre velocity of the outer planet is

$$v_{\text{peri},2} = \sqrt{\mathcal{G}M_{\star}(1+e_2)/a_1}, \quad (2)$$

M_{\star} being the mass of the star and e_2 the eccentricity of the outer planet. Treating the encounter between the two planets as a two-body scattering event, the relative velocity “at infinity” (i.e., close to the pericentre of the outer planet, before the planets’ mutual gravity becomes significant) is therefore

$$v_{\infty} = \sqrt{\mathcal{G}M_{\star}(1+e_2)/a_1} - \sqrt{\mathcal{G}M_{\star}/a_1}. \quad (3)$$

This velocity is shown in the space of (a_1, a_2) (where $a_1 < a_2$) in the left-hand panel of Figure 2. In extreme cases, of the inner planet being located at a few hundredths of an au, extreme relative velocities of $v_{\infty} > 100 \text{ km s}^{-1}$ are attainable. For planets at 0.1 au, $v_{\infty} > 20 \text{ km s}^{-1}$ can be attained. This is already almost twice Earth’s escape velocity ($v_{\text{esc},\oplus} \approx 11 \text{ km s}^{-1}$). Note that the velocity estimated here is a *minimum* for the v_{∞} of the planets’ encounter: the addition of radial or vertical velocity components (if the pericentre of the outer planet’s orbit lies inside the orbit of the inner planet, or if there is a mutual orbital inclination) will increase v_{∞} further.

How widely-separated may the orbits of planets initially be while still permitting eventual collision? This depends greatly on the underlying cause of instability in the system. In this Paper we consider two classes of system: tightly-packed systems which are intrinsically unstable, and intrinsically stable inner systems which are destabilised by the excitation of eccentricities in outer bodies (beyond ~ 1 au) by planet–planet scattering or Kozai perturbations

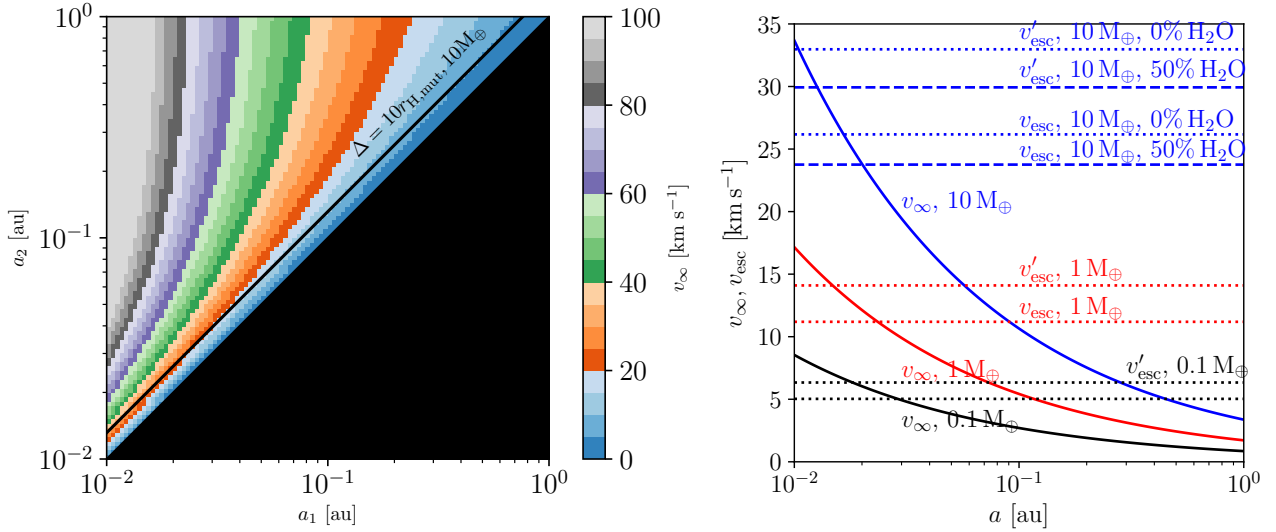


Figure 2. **Left:** Relative velocity at infinity if an outer planet at semimajor axis a_2 collides at pericentre with an inner planet on a coplanar circular orbit at a_1 . We also show the line $a_2 = a_1 + 10r_{\text{H,mut}}$ to mark the semimajor axis of an outer planet spaced 10 mutual Hill radii from the inner, when both planets have masses $10 M_{\oplus}$. **Right:** Relative velocity at infinity for two planets spaced 10 mutual Hill radii when the planet masses are both 0.1, 1 or $10 M_{\oplus}$ (solid lines). We also show (dotted/dashed lines) the single-planet surface escape velocity v_{esc} and the mutual escape velocity v'_{esc} , for Mars-like composition for $0.1 M_{\oplus}$ planets, Earth-like composition for $1 M_{\oplus}$ planets and for two compositions for $10 M_{\oplus}$ planets. Encounter velocities at infinity are a significant fraction of the escape velocity at $a \lesssim 1$ au. Gravitational focusing will boost the actual impact velocity significantly above escape velocity.

from a binary companion. In the former case, consider several planets separated by $\Delta r_{\text{H,mut}}$, where Δ is the spacing measured in units of the mutual Hill radius

$$r_{\text{H,mut}} = \frac{a_1 + a_2}{2} \left(\frac{M_1 + M_2}{3M_{\star}} \right)^{1/3}, \quad (4)$$

where M_i are the masses of the two planets. Instability in these systems is thought to be driven by the overlap of three-body mean motion resonances (Quillen 2011), and the timescale for instability is a sensitive function of Δ (e.g., Chambers et al. 1996; Faber & Quillen 2007; Smith & Lissauer 2009; Mustill et al. 2014), and systems of five Earth-mass planets are unstable within a few billion orbits at least out to separations of $\Delta = 9$ (Smith & Lissauer 2009). We mark the a_2 corresponding to a separation $\Delta = 10$ for $10 M_{\oplus}$ planets as a solid black line on the left-hand panel of Figure 2. We find *minimum* encounter velocities v_{∞} of over 30 km s^{-1} at a few hundredths of an au. In the right-hand panel of Figure 2 we show this encounter velocity as a function of a_1 , for Mars-mass, Earth-mass, and $10 M_{\oplus}$ planets. We also show the escape velocity of these planets in two forms: the single-planet surface escape velocity

$$v_{\text{esc}} = \sqrt{2GM/R}, \quad (5)$$

which is appropriate for the escape of a massless particle from the planet's surface, and the 2-planet mutual escape velocity as defined by LS12

$$v'_{\text{esc}} = \sqrt{2GM'/R'} \quad (6)$$

where M' is the combined mass of the two planets and R' is the radius of a sphere of the same total mass and density as the two planets. This latter is the appropriate measure for determining the outcome of a collision between comparable-mass bodies, and for equal-mass, equal-density planets is greater than the single-planet escape velocity by a factor $2^{1/3}$. For the calculation of the escape velocity of the $10 M_{\oplus}$ planets, we use the mass–radius relation of Valencia et al. (2007) for two compositions (0% water and 50%

water); the Mars-mass and Earth-mass planets have escape velocities of their Solar System archetypes. The minimum v_{∞} exceeds the escape velocity within ~ 0.02 au. However, as mentioned previously, the impact velocity will be enhanced by additional components of the velocity vector and by gravitational focusing. Numerical experiments by Volk & Gladman (2015) found that in intrinsically unstable systems such as those we are considering, the collision velocities (particularly those following the first collision) easily exceed twice the escape velocity.

Systems destabilised by external influences, however, can be expected to be excited to higher eccentricities and therefore higher encounter velocities. The terrestrial planets of the Solar System have a small chance of experiencing an instability driven by the ν_5 secular resonance (Laskar & Gastineau 2009; Batygin et al. 2015). In this case, Mercury can be placed on a collision trajectory with Venus: a separation of 0.336 au, or 63 mutual Hill radii, requiring an eccentricity on Mercury's part of $e = 0.87$ if Venus retains a circular orbit. We have previously shown (Mustill et al. 2015, 2017) that systems of transiting planets can be destabilised by the action of dynamically-excited planets beyond 1 au. In these case, collisions can occur between widely-separated transiting inner planets, or between one of the inner planets and one of the outer planets if its eccentricity is sufficiently highly excited, placing these systems towards the upper left of the left-hand panel of Figure 2 with very high impact velocities of $\sim 100 \text{ km s}^{-1}$ to be expected, particularly if orbits become highly inclined or even retrograde. Other sources of instability that may result in high-velocity collisions would be in systems destabilised by secular inclination resonance sweeping, for example as a rapidly-rotating young star spins down (Spalding & Batygin 2016), where the inclination excitation could also lead to high relative velocities.

These arguments show that the collisional environment of close-in planets is extreme, and that the collisions that occur will often be significantly higher than the planets' escape velocity. Therefore, the usual assumption of perfect merging in N -body integrators will

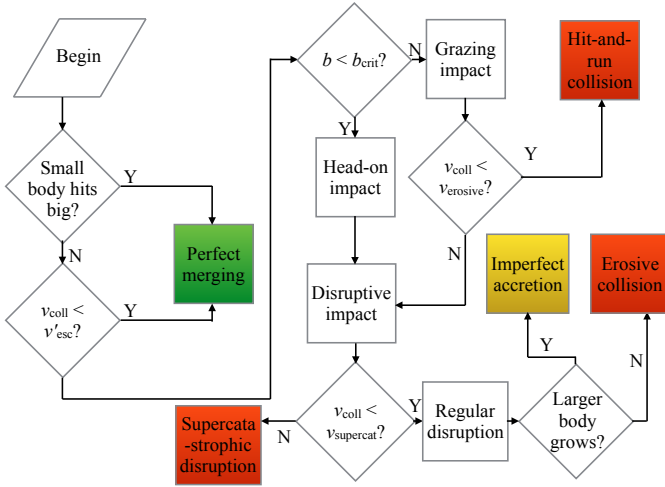


Figure 3. Flowchart illustrating the collision algorithm we implemented in the MERCURY code, based on [Leinhardt & Stewart \(2012\)](#). If the collision velocity is lower than the mutual escape velocity, the standard MERCURY perfect merging routines are called, whereby the bodies merge into one with the combined mass of both the original bodies; this also occurs if a small body in MERCURY (a massive test particle) strikes a big body. If the collision velocities exceed this threshold, we check for grazing collisions (if the impact parameter is above a critical value, so that the centre of mass of the smaller body misses the larger). These lead to a hit-and-run outcome with minimal mass loss, if the impact velocity is below the erosion threshold. Head-on impacts or higher-velocity grazing impacts lead to disruptive outcomes: here the larger body may still grow, with some mass lost to collisional debris (imperfect accretion), it may lose mass (erosion), or it may experience a supercatastrophic collision at very high impact velocities. See Section 3.1 for further details. The colour coding of outcomes (green for perfect merging, yellow for imperfect accretion, and red for erosion) corresponds to the bars in Figures 4, 6 and 8.

no longer be valid. We now proceed to numerically study how common outcomes other than perfect merging are, with a modified MERCURY N -body code. We describe the implementation of the collision algorithm in the next section, before proceeding to study the collision statistics in intrinsically unstable systems, and then those destabilised by outer bodies. Finally, we study the effects on *in-situ* formation of rocky transiting planets.

3 THE COLLISION MODEL

We adjust the MERCURY N -body integrator to better handle high-velocity collisions in the following way. First, we alter the routines checking for a collision between bodies. In MERCURY this check is performed by an interpolation of particle trajectories within each time-step to see whether an intersection has taken place. We need to know, in addition, what the parameters of the collision are (collision velocity and impact parameter), not merely whether or not one has occurred. Therefore, if a collision is detected, we rerun the integration from the start of that timestep for half of the duration of the timestep. This is repeated iteratively until the timestep falls to 10^{-5} days, thus providing accurate values for the impact parameter and velocity. As collisions are relatively infrequent, the computational cost of this is negligible.

Next we change the outcomes of the collisions themselves. We base our algorithm on that of LS12, suitable for collisions between rocky protoplanets or planets. We are therefore studying genuine

“super-Earths” rather than “mini-Neptunes” which have a significant gaseous component, a distinction which seems to occur at around $1.5 R_{\oplus}$ ([Weiss & Marcy 2014](#); [Fulton et al. 2017](#)). The collision algorithm takes as input the masses and radii (and hence densities) of the two bodies, and the impact parameter b and the collision velocity v_{coll} (both of these *at the moment of impact*, not at a point at infinity). From these inputs, collisions are classified into perfect merging (small v_{coll}), hit-and-run (large b but not enough v_{coll} for disruption), disruptive (moderately large v_{coll} ; some material lost from the two planets, while the larger may accrete some material or be eroded) and super-catastrophic (very large v_{coll} ; less than 10% of the total mass remains bound in largest remnant). The algorithm is described in detail in the next subsection.

In the case of disruptive and hit-and-run collisions, mass is lost from one or both of the planets. Some rock is vapourised, and a fraction of this will recondense into small dust grains. Other ejecta will be thrown off as large, gravitationally-bound chunks. We treat the debris as small bodies in MERCURY: super-particles which have mass, interact gravitationally and collide with the big bodies but have no direct interactions with each other. This approach means that, as far as purely gravitational forces go, we can neglect uncertainties in the size distribution of the debris. However, the debris is also subject to collisional processing and radiation forces ([Burns et al. 1979](#); [Wyatt et al. 2007](#); [Jackson & Wyatt 2012](#)) which can significantly reduce its lifetime. Due to the complexities of modelling the initial size distribution of collisional debris and its subsequent evolution, we consider two extreme cases: for most of our simulations, we simply remove the debris instantaneously from the simulations. This represents the case where the debris is primarily in the form of small grains or vapour and is removed on dynamical time-scales by the stellar wind and radiation forces, or else is rapidly collisionally ground down to such small sizes. We discuss this in more detail in Section 7.2. For some simulations, we retain 100% of the debris as small bodies in MERCURY. This represents the opposite extreme in which most of the mass of the debris is in a few large fragments. Reality will lie somewhere between these two scenarios.

3.1 The collision algorithm

The collision algorithm we implement is shown schematically in Figure 3 and described below:

(i) **Remove small bodies involved in a collision.** If a large body collides with a small body (as defined by MERCURY: small bodies are massive test particles) then perfect merging is assumed.

(ii) **Calculate the interacting mass m_{interact} :** the mass of the fraction of the projectile whose trajectory intersects the target. This fraction is calculated approximately in LS12, Equation 10. However, we found that this formula was not always accurate, particularly when the projectile and the target were of comparable radii, and we evaluate the interacting mass by numerical quadrature in all cases. We also account for the possibility of a less massive but geometrically larger “projectile” of low density.

(iii) **Calculate the mutual escape velocity $v_{\text{esc}} = \sqrt{2M'/R'}$** (LS12 Equation 53). We slightly change the definition of M' and R' compared to LS12: we set $M' = M_1 + M_2$ not $M_1 + m_{\text{interact}}$ as all the mass of the two bodies interacts gravitationally, and we set $R' = (3(M_1/\rho_1 + M_2/\rho_2)/(4\pi))^{1/3}$ to account for the projectile and the target potentially having different densities. Defining the mutual escape velocity in this way allows us to treat as perfect mergers hit-and-run impacts that later merge ([Genda et al. 2012](#)),

although there is a slight dependence on impact parameter that we do not capture.

(iv) **If the collision velocity $v_{\text{coll}} \leq v'_{\text{esc}}$ then a perfect merger occurs.** Note that the mutual escape velocity is defined for a spherical configuration of matter, whereas when the two planets make contact they are in a dumbbell-shaped higher-energy configuration. Therefore, two bodies at rest at infinity will not have reached their mutual escape velocity at the moment of impact, and so collisions at velocities less than the mutual escape velocity are possible.

(v) **Determine whether a grazing impact occurs.** If the trajectory of the centre of mass of the less massive body does not intersect the target, the impact is counted as grazing.

(vi) **Calculate the threshold for an erosive collision in which the larger planet loses mass.** We set $M_{\text{lr}} = M_{\text{target}}$ in LS12 Equation 5.

(vii) **Determine whether a hit-and-run collision has occurred.** This occurs if the impact velocity is below the erosion threshold and the collision is grazing. If a hit-and-run collision occurs then jump to (xii).

(viii) **Calculate the threshold for super-catastrophic disruption.** This is given by LS12 Equation 5 with $M_{\text{lr}} = M_{\text{tot}}/10$.

(ix) **Determine the class of collision outcome: imperfect accretion, erosion or supercatastrophic disruption.** This depends on the impact velocity compared to the computed thresholds.

(x) **Calculate the largest remnant mass.** This is given by LS12 Equation 4 for regular disruption, and LS12 Equation 44 for supercatastrophic disruption. We do not preserve the *second-largest remnant* as a separate big body, since its mass is usually $< 10\%$ of the initial mass of the smaller body (LS12 Equation 37).

(xi) **Assign new velocity to the largest remnant.** In this we follow the procedure in Section 3.3 of LS12 if the mass of the largest body decreases. If the mass increases, this may not conserve momentum, and we therefore add to the larger body's momentum that of the material accreted from the smaller body.

(xii) **Determine outcome of hit-and-run collisions.** The algorithm of LS12 does not specify the amount of mass lost in a hit-and-run collision. However, a small fraction of mass is indeed lost. We approximate this with a geometrical approach where the material in the overlap region calculated in step (ii) is removed. In our fiducial runs described below, the median mass removed in a hit-and-run collision was 2%, although some result in greater mass loss (90% lost less than 16%).

(xiii) **Distribute mass lost into small-body fragments if desired.** A fraction f_{remove} of the mass lost in the collision is instantaneously removed from the simulation. This is to represent material which is vapourised and, after recondensing, will be removed from the system on a short time-scale by radiation forces. The remainder of the material is distributed into fragments, modelled as small bodies in MERCURY. As these are super-particles, we distribute the mass equally amongst them. To prevent an excessive number of fragments being generated and slowing down the simulations, we spawn 10 particles per collision. We set $f_{\text{remove}} = 1$ for most of this paper.

(xiv) **Assign velocities to fragments.** Following Jackson & Wyatt (2012), who fit one simulation outcome from Marcus et al. (2009) for the Moon-forming collision, we assign fragments velocities with a truncated Gaussian distribution. We spawn the fragments at the edge of its Hill sphere with an isotropic distribution, and scale the velocity distribution by the planetary escape velocity.

(xv) **Adjust velocity of largest remnant to conserve momentum.** If fragments are generated, we adjust the momentum of the largest remnant after assigning velocities to the collision fragments.

4 NUMERICAL STUDY I: INSTABILITY AMONGST THE INNER PLANETS

4.1 Setup

We first turn to purely internal instabilities, of the kind studied by Johansen et al. (2012), Pu & Wu (2015), Volk & Gladman (2015) and Izidoro et al. (2017). We set up tightly-packed systems of five super-Earths (masses drawn logarithmically from $1 - 10 M_{\oplus}$) and evolve them for 10 Myr with both the perfect merging assumption and the LS12 algorithm. We run four sets with each collision prescription, with the innermost planet being placed at 0.1, 0.3, 0.5 or 0.7 au. We also run sets with the innermost planet at 0.1 au for planetary mass ranges $0.1 - 1 M_{\oplus}$ and $0.3 - 3 M_{\oplus}$. Planets are separated by 4 – 6 mutual Hill radii, which ensures dynamical instability on short timescales (from a few 100 yrs onwards). We also test more widely-spaced but still unstable systems to verify that the results are not sensitive to the initial separation, running simulation sets at 0.1 au with initial separations of 6 – 8, 7 – 9 and 8 – 10 mutual Hill radii. Most simulations start with planets' inclinations drawn from 0° to 5° of the reference plane, which provides a typical mutual inclination of $\sim 3^{\circ}$ (Johansen et al. 2012). To test the effects of the initial inclination distribution, we also run simulations from a flatter initial configuration with inclinations drawn from 0° to 0.1° .

Our fiducial case has the innermost planet at 0.1 au, masses in the range $1 - 10 M_{\oplus}$, separations from 4 – 6 mutual Hill radii, and inclinations up to 5° .

4.2 Results

The outcomes of collisions are summarized in Figure 4. The upper panels show a broad breakdown of collision outcomes into perfect mergers, accretion at less than 100% efficiency, and erosive or disruptive collisions where the mass of the largest planet decreases. The majority of erosive collisions are grazing impacts which result in a relatively small fraction of mass lost. The lower panels show the detailed distributions (as kernel density estimates and cumulative distributions) of the mass change in each collision in each simulation set, normalised to the mass of the larger planet. In the left-hand column we vary the innermost planet's semimajor axis, in the centre column the range of planetary masses, and in the right-hand column the planetary spacing.

The upper panels show that most collisions very close to the star do not result in perfect merging: only 42% of collisions in the 0.1 au simulations resulted in perfect merging. We see a trend towards more gentle collisions as we move away from the star: in the simulations at 0.7 au, the fraction of perfect mergers has risen to above 60%. The mass of the planets has a very strong effect, with only 26% of collisions resulting in perfect mergers when the planetary masses are in the range $0.1 - 1 M_{\oplus}$. These trends are expected from a consideration of planetary orbital and escape velocities, as discussed in Section 2: in a fixed planet mass range (escape velocity), decreasing the distance to the star increases the Keplerian and therefore the collision (v_{∞}) velocities, while at a fixed semimajor axis, decreasing the mass decreases the escape velocity but keeps the Keplerian velocity constant. Nevertheless, the erosive nature of collisions between the smaller planets on short-period orbits may pose a challenge to models of *in-situ* formation from lower-mass planetary embryos (e.g., Hansen & Murray 2012, 2013; Chatterjee & Tan 2014; Schlichting 2014; Moriarty & Fischer 2015; Ogihara et al. 2015; Moriarty & Ballard 2016), and we investigate this more thoroughly in Section 6. Finally, we see essentially no dependence

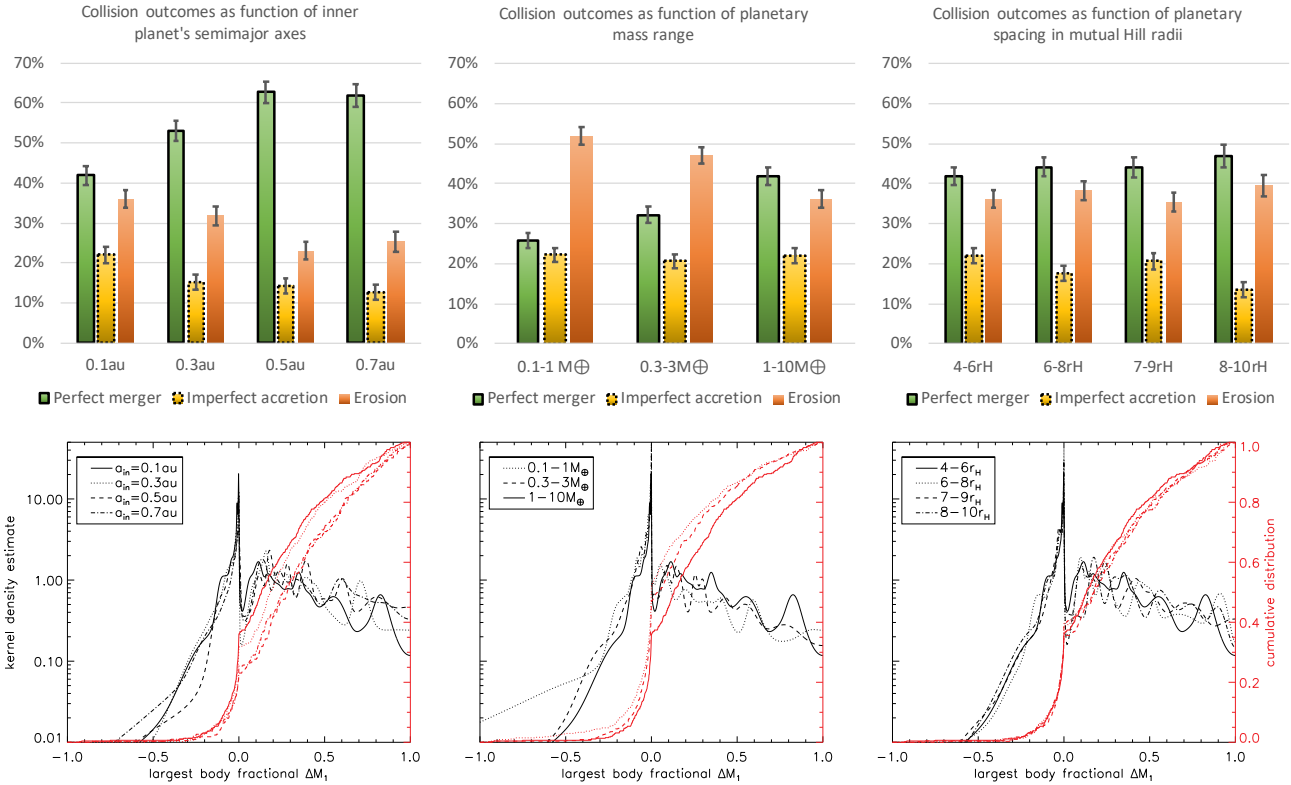


Figure 4. Outcomes of collisions in unstable systems of five planets. The fiducial system has planets with masses $1 - 10M_{\oplus}$, spaced by $4 - 6$ mutual Hill radii, with the innermost planet at 0.1 au; we vary one parameter per column of panels. The upper panels show the broad breakdown of collision outcomes, with each set of three bars representing a set of 100 simulations. Collisions are divided into perfect merging (both planets merge with no mass loss), imperfect accretion (larger planet grows but does not accrete 100% of the mass of the smaller planet), and erosion (larger planet loses some mass; this includes hit-and-run impacts). The lower panels then show the distributions of the fractional change in mass for the largest planet in the collision ($\Delta M_1/M_1$). Kernel density estimates are shown in black against the left-hand vertical axis, while the cumulative distributions are shown in red against the right-hand axis. The large spike of slightly-erosive collisions is largely due to hit-and-run impacts, which result in a small amount of mass loss. **Left:** The effects of changing the planets’ semimajor axes. The innermost planet is placed at 0.1 , 0.3 , 0.5 or 0.7 au; masses are $1 - 10M_{\oplus}$. We find a higher fraction of erosive collisions closer to the star, as expected from the higher Keplerian (hence impact) velocities. However, even at 0.1 au, most collisions remain accretional. **Centre:** The effects of changing the mass of the planets. The innermost planet is always at 0.1 au; masses are in the range indicated in the legend. The smaller planets experience a higher fraction of erosive collisions, as expected from their lower surface escape velocities. **Right:** The effects of changing the planets’ initial separations in mutual Hill radii. The initial separation in mutual Hill radii for the planets is set to the ranges $4 - 6$, $6 - 8$, $7 - 9$ and $8 - 10r_{H,\text{mut}}$. The initial spacing has no noticeable effect on the distribution of collision outcomes. In each panel there are 100 runs in each set of integrations.

of collision outcomes on the initial spacing of the planets. Increasing the spacing increases the time-scale for the onset of collisions, but it does not affect the velocities once collisions begin.

In the lower panels of Figure 4 we show in detail the distribution of mass changes to the largest planet. While many collisions are erosive, many of these are in fact hit-and-run collisions resulting in little mass loss, seen as the large spike in the kernel density estimate just below $\Delta M = 0$. Only a few percent of collisions result in the larger planet losing more than 10% of its pre-impact mass. In total, 7 – 11% of the total initial mass of the planets in the runs at 0.1 au with planets in the $1 - 10$ Earth mass range was lost, slightly lower in the more widely-spaced systems which experienced fewer collisions. This fraction is considerably higher when starting from lower-mass planets: 19% in the $0.3 - 3$ Earth mass range and 25% in the $0.1 - 1$ Earth mass range.

In Figure 5 we show the final numbers of planets in the systems. The systems typically reduce to 2-planet systems; the more widely-spaced ones have more planets surviving at the end, but may reduce further if integrated for longer. For the simulation sets where the final planet mass can be below $1M_{\oplus}$ (any with the LS12 collision

model, and any with initial planet masses below $1M_{\oplus}$), we show separately the numbers of planets with mass $> 1M_{\oplus}$, as a crude criterion for detectability by *Kepler*. For most simulation sets, there is little difference in the final multiplicities when comparing the perfect merging prescription with LS12. This is true even when including “undetectable” planets smaller than $1M_{\oplus}$. The exceptions to this are when starting from smaller planets: we then see significant differences in the numbers of planets that survive with mass greater than Earths between the two collision models: for the $0.1 - 1M_{\oplus}$ simulations, we find with perfect merging 20% of systems having zero detectable planets, 70% having one, and 10% having two; with the LS12 algorithm, these numbers become respectively 40%, 57% and 3%.

For the runs discussed so far, we have assumed an initial inclination distribution of up to 5° , meaning that the mutual inclinations peak at around 3° (Johansen et al. 2012). We now study the effects of starting from initially flatter systems, with inclinations only up to 0.1° (Figure 6). Here we find a larger fraction of perfect mergers as collision outcomes at small orbital radii: 65% in the flat systems at 0.1 au spaced $4 - 6$ mutual Hill radii, compared to 42% in the

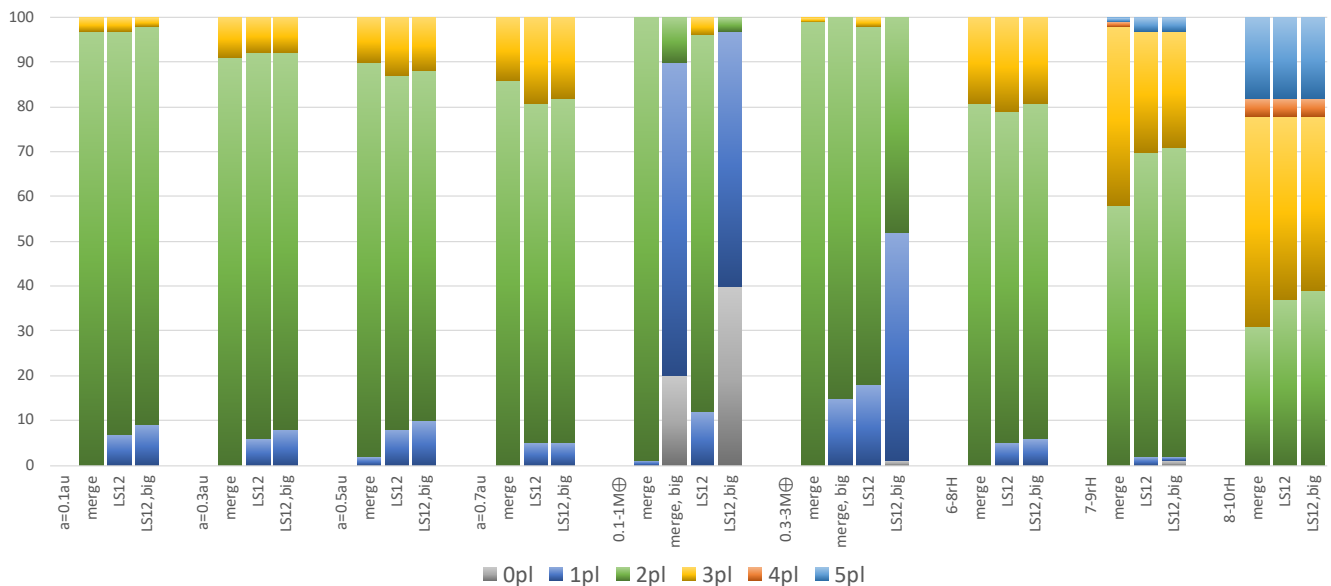


Figure 5. Final multiplicities of the initially 5-planet systems of Figure 4. Outcomes are shown as a function of semimajor axis (first four sets), mass (fifth and sixth sets), and initial orbital spacing in mutual Hill radii (final three sets). Each set of simulations is run both with the standard MERCURY collision algorithm where collisions always result in perfect mergers (“merge”), and with our more realistic algorithm (“LS12”). In columns labelled only “merge” and “LS12”, we count all planets; in columns labelled “... , big” we count only planets of at least $1 M_{\oplus}$. Most systems reduce to 2-planet systems, or 3-planet systems for the initially more widely separated ones. When counting only planets at least as massive as Earth, many zero- or single-planet systems form when the initial planet masses are small. This is exacerbated when using the realistic collision model.

inclined systems. However, here there is a dependence on planetary spacing, and for the systems spaced 8 – 10 mutual Hill radii the fractions more closely resemble the ones from the inclined systems: 53% perfect mergers and 31% erosive. Here, the wider systems have more time in which to become dynamically excited, with a final mean inclination of 2.6° for the most widely-spaced set compared to 1.9° for the tightest set.

Finally, in Figure 7 we show the separations of surviving two-planet systems in the runs initially at 0.1 au. In the top panel we show the separations in mutual Hill radii. The runs with the LS12 collision algorithm result in much more widely-separated two-planet systems than those run with the perfect merging algorithm, and in fact the distribution more closely resembles the observed separations of *Kepler* multi-planet systems which peaks at ~ 20 mutual Hill radii (Weiss et al. 2017). In the lower panel we show the period ratios in the same systems. With the LS12 algorithm, we find a marked (4σ) deficit around a period ratio of 2, possibly associated to the 2:1 mean motion resonance (MMR); this feature persists independent of the bin size. This feature may arise because resonant and near-resonant orbits are less stable in the systems resulting from the LS12 runs than in those run with perfect merging: the planets in the former have a slightly higher mean eccentricity (0.13 versus 0.08) which could render the resonances less stable. This may contribute to the observed lack of *Kepler* planets in MMRs (Lissauer et al. 2011; Fabrycky et al. 2014), although to establish this would require a treatment of tidal eccentricity damping (e.g., Delisle & Laskar 2014) and the damping from collisional debris (similar to the planetesimal damping considered by Chatterjee & Ford 2015), both of which could result in small changes to the planets’ semimajor axes that might affect this feature.

5 NUMERICAL STUDY II: INSTABILITY INDUCED BY OUTER DYNAMICS

In this section, we investigate the effects of changing the collision model to the instabilities induced by an outer system, as studied by Mustill et al. (2017). As discussed in Section 2, we expect that collisions will be more violent in these systems due to the large orbital eccentricities that external perturbers can excite.

5.1 Setup

In Mustill et al. (2017) we studied two dynamical scenarios: an inner system together with an outer system of planets unstable to planet–planet scattering (GIANTS), and an inner system together with a single outer planet and a wide binary stellar companion BINARIES. In either case, the excitation of eccentricity of the outer planet(s) can lead to its pericentre approaching or overlapping the orbits of the inner planets. In roughly 1 in 4 of these simulations, the inner system was destabilised by the outer system, losing one or more of the inner planets. Planet–planet collisions accounted for around half of the planets lost from the inner system (43% in BINARIES, and 51% in GIANTS).

Motivated by the results of Mustill et al. (2017), we run simulations of three-planet systems with extra bodies in the outer system. For our inner architectures, we depart from the setup of Mustill et al. (2017), who took actual triple-planet *Kepler* systems as a template, as planets in these systems often have a significant gaseous component. Instead, we removed the second and fourth planets from the quintuple systems we constructed for Section 4, leaving highly-spaced triple-planet systems.

We construct two sets of systems with different outer system architectures. For the first set (3p+3J), we add three Jupiter-mass planets with the innermost at 1 au and the others separated by 4 – 6

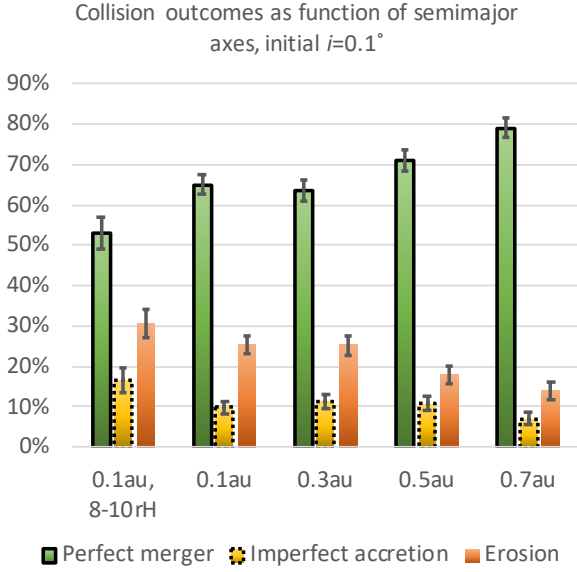


Figure 6. Collision outcomes when starting from a flat configuration with initial inclinations in the range 0° to 0.1° (compare to left-hand panels of Figure 4, where the inclinations were up to 5°). Initial spacings are all 4 – 6 mutual Hill radii except for the leftmost set, spaced at 8 – 10 mutual Hill radii. In most of these flat systems, a larger fraction of collisions result in perfect mergers than in the initially more inclined systems shown in Figure 4, although the more widely-spaced systems ($8 - 10r_{H,\text{mut}}$) have statistics comparable to their more inclined counterparts.

mutual Hill radii. Using equal-mass planets ensures very strong scattering that will be very disruptive for the inner system and efficiently excite eccentricities (Carrera et al. 2016; Huang et al. 2017). For the second set (3p+J+B) we add a single Jupiter-mass planet at 1 au, and a Solar-mass binary at 40 au (the peak of the period distribution for Solar-type stars, Duchêne & Kraus 2013) with an eccentricity of 0.2 and an inclination of 50° , sufficient to drive Kozai cycles on the giant planet, but that restricts the planet’s pericentre from sweeping through the entire inner planetary system and destroying all planets. We compare these systems to the fiducial 5-planet systems at 0.1 au from Section 4, which we refer to as 5p in this section.

5.2 Results

The frequency of collision outcomes, and the distributions of the changes to the mass of the largest body, are shown in Figure 8. We also show on these plots the statistics from our fiducial self-unstable 5-planet simulation set (at 0.1 au and with separations of $4 - 6r_{H,\text{mut}}$). For these runs including outer planets, we only include in the statistics collisions where both of the planets were members of the inner triple system (or their collisionally accreted or eroded descendants), as the collision prescription we use is calibrated for rocky, not gaseous, planets.

The systems destabilised by the external planets experience far more erosive collisions than the self-unstable systems: only 20 – 30% of the collisions in these runs resulted in perfect mergers, while 50 – 60% were erosive. This compares to the $\sim 35\%$ erosive collisions in the self-unstable systems. Individual erosive impacts are often more destructive: we find 2.4% and 0.8% supercatastrophic disruptions in 3p+3J and 3p+J+B compared to only 0.4% in the

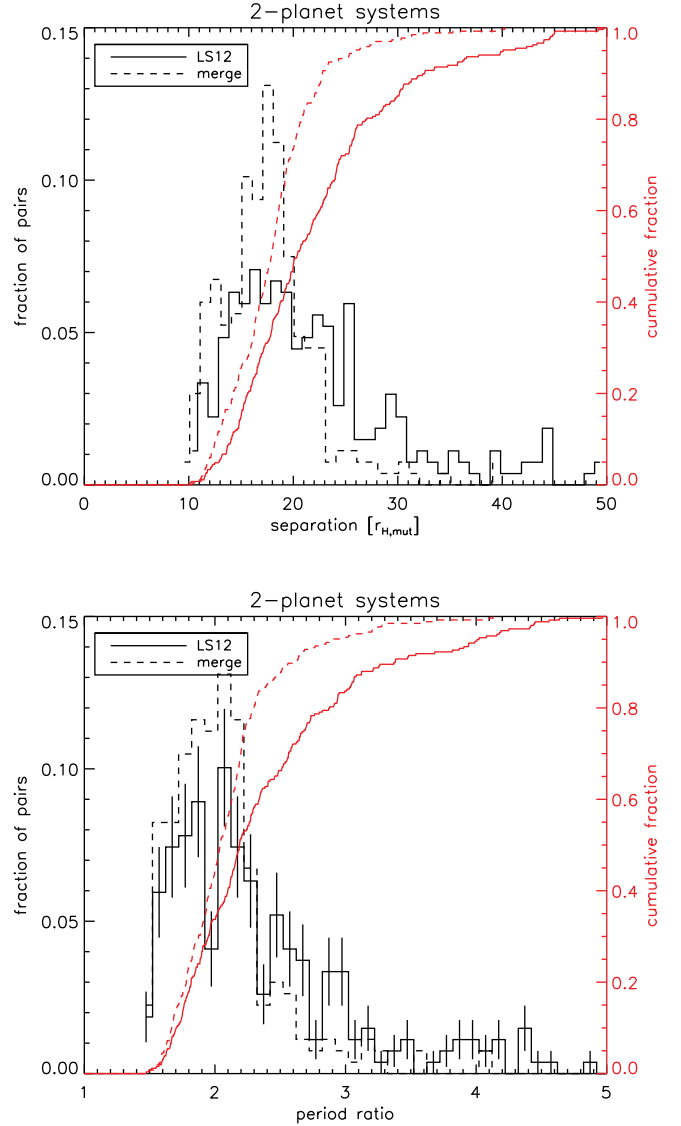


Figure 7. Separations of planets in systems ending with two planets. Systems initially had their inner planet at 0.1 au, with masses in the range $1 - 10M_\oplus$, and we include all initial separations. Simulations run with the LS12 collision algorithm are shown as a solid line, and those with standard perfect merging as a dashed line. The right-hand axes show the cumulative distribution. **Top:** Separations in mutual Hill radii. Assuming that all collisions result in perfect merging yields a narrower and tighter range of final orbital separations. **Bottom:** Period ratios in the same systems. 1σ Poisson error bars are marked on the solid histogram. A marked $\sim 4\sigma$ deficit of planets near the 2:1 mean motion resonance is found when using the improved collision algorithm.

set 5p. In systems which experienced collisions between the inner planets, 13.8% of the total planetary mass was lost in collisions in 3p+3B and 21.8% in 3p+J+B, compared to only 11.4% in 5p. However, even in the extreme case of the binary-perturbed 3p+J+B systems, the final distributions of planet masses in the destabilised systems are not statistically distinguishable ($p = 0.29$ on a KS test, albeit with only around 30 planets in each sample).

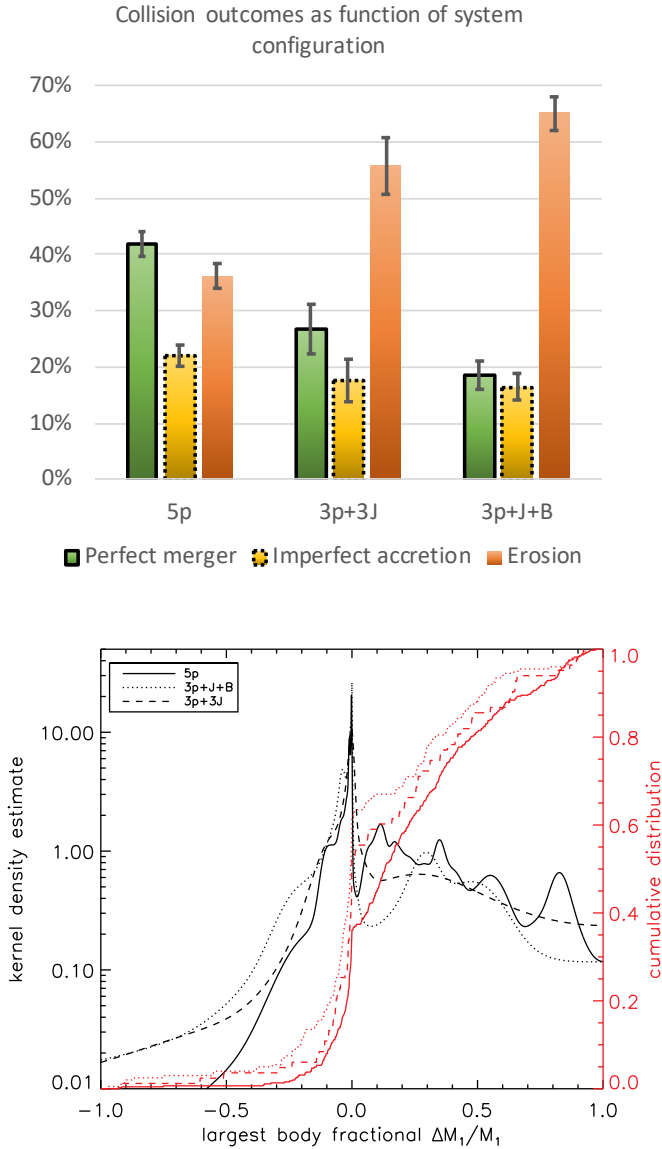


Figure 8. Collision outcomes of self-unstable systems (5p: the set of runs at 0.1 au from Section 4), compared to those destabilised by dynamically active outer systems: giant planets undergoing Kozai perturbations (3p+J+B) and scattering (3p+3J). **Top panel:** broad classification of collision outcomes. **Bottom panel:** distribution of changes to largest body mass in the collisions. Planets in systems destabilised externally experience even more violent collisions than those systems that are intrinsically unstable.

6 NUMERICAL STUDY III: *IN-SITU* PLANET FORMATION FROM EMBRYOS

Motivated by the decreasing prevalence of perfect mergers at lower planet masses, we now study the effects of changing the collision prescription on *in-situ* formation of super-Earths from rocky embryos. While several authors have now considered the effects of adopting a more realistic collision prescription in the formation of the terrestrial planets (Chambers 2013; Carter et al. 2015; Leinhardt et al. 2015; Chambers 2016; Quintana et al. 2016), studies of similar formation processes for close-in planets have so far mostly modelled collisions as perfect mergers (Hansen & Murray 2012, 2013;

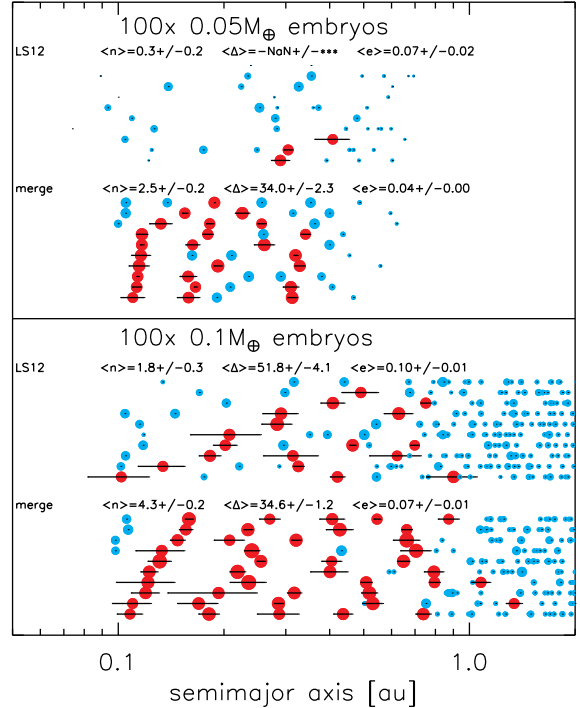


Figure 9. Effects of the collision algorithm on planet formation from Mars-sized embryos. In the upper panel we start with 100 $0.05 M_{\oplus}$ embryos; in the lower, 100 $0.1 M_{\oplus}$ embryos. Systems are shown after 10 Myr of evolution, by which point planet formation is still ongoing beyond ~ 1 au but has completed within a few tenths of an au. Symbol size is proportional to the cube root of mass, and planets more than at least $1 M_{\oplus}$ are in red, those smaller (whether embryos or fragments) in blue. Eccentricities are shown for the planets over $1 M_{\oplus}$ as horizontal lines. The lower set of systems in each panel are run with perfect merging, the upper set with the LS12 collision prescription with fragments instantly removed. For each set, we show the mean number of planets at least Earth's mass, and the mean separations (in mutual Hill radii) and eccentricities of these planets (error bars show standard errors on the means). Perfect merging results in high-multiplicity systems; LS12 with fragments removed results in more widely-spaced, lower multiplicity systems, and when starting from the smaller embryos, planet formation is almost entirely suppressed.

Chatterjee & Tan 2014; Schlichting 2014; Moriarty & Fischer 2015; Ogihara et al. 2015; Moriarty & Ballard 2016; Izidoro et al. 2017; Matsumoto & Kokubo 2017, but see Wallace et al. (2017) for an exception). This is despite the fact that the assumption that collisions always result in perfect merging becomes worse as one moves closer to the star, as we showed above. Here, we explore the effects of adopting the more realistic collision model.

We run simulations with 10 Earth masses of material in 100 $0.1 M_{\oplus}$ embryos, with the innermost placed at 0.1 au and embryos spaced by 4 – 6 mutual Hill radii. This sets the outermost embryo at around 1.7 – 1.9 au. Initial inclinations are up to 0.1° . We run these simulations for 10 Myr with either the perfect merging algorithm, and with the improved algorithm based on LS12 with all collision fragments removed. We furthermore run sets of simulations starting from 100 smaller $0.05 M_{\oplus}$ embryos. There were 10 simulations in each set.

Simulation results are shown in Figure 9. Each row shows the semi-major axes of bodies in a single system. Red symbols show

planets of at least one Earth mass, with horizontal bars showing the eccentricities of these large objects. By the end of the simulation at 10 Myr, planet formation is complete out to ~ 1 au.

With the larger $0.1 M_{\oplus}$ embryos, when run with perfect merging, a large number of Earth-mass bodies form, out to around 1 au (where planet formation is still ongoing). The final systems have a mean of 4.3 planets per system, separated by a mean of 35 mutual Hill radii. This changes markedly if run with the LS12 algorithm, removing collision fragments: in these systems, an average of only 1.8 planets more massive than Earth form, and the multiple systems are more widely spaced (mean of 52 mutual Hill radii). We formed three intrinsic singletons and one intrinsic “planetless” star (its largest planet was $0.82 M_{\oplus}$). These simulations lost 33% of all their material, and 41% of material within 1 au. We also tested the effects of retaining the collision fragments in these systems. In these cases, fragments were quickly reaccreted, and the multiplicities of systems were again high (a mean of 3.4 planets more massive than Earth).

The effects of the LS12 algorithm are more pronounced when starting from the smaller ($0.05 M_{\oplus}$) embryos, owing to the higher impact velocities relative to escape velocities. When starting from one hundred $0.05 M_{\oplus}$ embryos with low inclinations, we formed one single-planet, three two-planet and six three-planet systems with perfect merging, but only three single-planet and seven zero-planet systems with LS12, removing the fragments. Adopting the more realistic collision algorithm can thus strongly curtail *in-situ* planet formation from small embryos, so long as the collisional debris is quickly removed from the system.

Our simulations transition rapidly from a majority forming no planets (when starting from $0.05 M_{\oplus}$ embryos) to a majority forming multiple planets (starting from $0.1 M_{\oplus}$ embryos). Although we suffer from small-number statistics, this may suggest a critical embryo mass above which embryos at ~ 0.1 au can avoid collisional grinding and consistently grow to larger planets. It may also raise a fine-tuning problem with this model, since one interpretation of the statistics of transit multiplicities from the *Kepler* mission is that half or more of planetary systems contain only one planet within ~ 1 au (e.g., Johansen et al. 2012; Ballard & Johnson 2016), although this interpretation is not unique (see e.g., Zhu et al. 2018, who favour a larger fraction of multiple systems whose observed transit multiplicities are reduced by inclination excitation).

We note that a recent study by Wallace et al. (2017) found that fragmentation does *not* impede the formation of rocky planets on short orbital periods. Wallace et al. (2017) used a collision prescription similar to ours, also based on the results of Leinhardt & Stewart (2012), with some minor differences in the treatment of hit-and-run collisions. The major difference, however, is in the treatment of smaller collision fragments: while we remove these, Wallace et al. (2017) retained them, with the qualification that objects could not be reduced below a “Minimum Fragment Mass”. As we discuss in Section 7.2 below, we expect most fragments to be ground to smaller sizes in a collisional cascade, and then removed by radiation forces, before they re-accrete onto one of the larger planets. By imposing a Minimum Fragment Mass, Wallace et al. (2017) did not capture this collisional cascade. Our study and that of Wallace et al. (2017) thus represent the two extreme cases of no mass removal and instant mass removal. Further study would require collisional modelling of the debris fragments within the N -body simulations, but we suspect that reality would lean more towards our implementation at smaller orbital distances (~ 0.1 au) and more towards that of Wallace et al. (2017) at larger orbital distances (~ 1 au), where orbital velocities

are lower, collisional velocities are lower, and gravitational focusing enhances re-accretion.

7 DISCUSSION AND CONCLUSIONS

7.1 Implications for the *Kepler* dichotomy

The “*Kepler* dichotomy” refers to the large number of systems possessing only one transiting planet compared to multiple systems (Johansen et al. 2012; see also Lissauer et al. 2011; Fang & Margot 2012; Tremaine & Dong 2012). Two possible causes of the excess of singles are formation (some systems just form with only one planet within a few tenths of an au) and later dynamical evolution (many or all systems form as multiples, and most are unstable and reduce to single-planet systems).

Attempts to reproduce the dichotomy through dynamical instabilities have met with mixed success. Mustill et al. (2017) and Huang et al. (2017) show the strong effects instabilities amongst outer planets can have on inner planets, but the relatively small occurrence rate of gas giants means that this can only make a modest contribution to the destabilisation of the population of transiting systems (in Mustill et al. 2017, we argued that $\lesssim 20\%$ of multiple systems will be destabilised by outer planets, with the uncertainty dominated by the poorly-constrained occurrence rate of sub-Jovian planets beyond 1 au). The recent work by Izidoro et al. (2017) finds that resonant chains of planets are frequently unstable, although still not frequently enough to match the *Kepler* data.

Our simulations show that the incorporation of an improved collision model does not have a significant effect on the multiplicities of systems after instability. Based on the weak sensitivity of collision outcomes to the initial spacings in our non-resonant 5-planet systems, we expect that the effects of changing the collision algorithm in unstable resonant systems will not be significantly different. We also do not form intrinsically zero-planet systems through continued grinding down of the planets, as hypothesised by Volk & Gladman (2015). Even when perfect merging is abandoned, most collisions between mature planets more massive than Earth do not result in enough mass loss to significantly affect the planetary mass distribution or the number of large, detectable planets.

Observed multiplicity is a function not only of a system’s intrinsic multiplicity but of the planets’ separations and mutual inclinations. Our systems evolved with the LS12 algorithm end up slightly more widely spaced and dynamically excited than those run with perfect merging. This has a moderate effect on observed multiplicities: taking the systems in our baseline simulations ($a = 0.1$ au), we clone the systems at the end of the simulation to generate a large sample of 10 000 systems and observe these from random orientations. The ratio of systems observed with two transiting planets to one transiting planet is 2.5 : 1 for the simulations with perfect merging and 3.4 : 1 for those run with the LS12 algorithm, despite the intrinsic multiplicities being almost identical. This falls far short, however, of the observed ratio of around 6:1 (e.g., Johansen et al. 2012; Lissauer et al. 2014).

The alternative explanation for the *Kepler* dichotomy—that it arises from the processes of planet formation—fares slightly better from our results. Previous attempts to explain the dichotomy through *in-situ* accretion of embryos have invoked a large range of surface density gradients in the planetesimal disc (Moriarty & Ballard 2016). In our simulations, when abandoning the assumption of perfect merging between embryos, a greater diversity of outcomes is seen than when retaining perfect merging, with many simulations forming

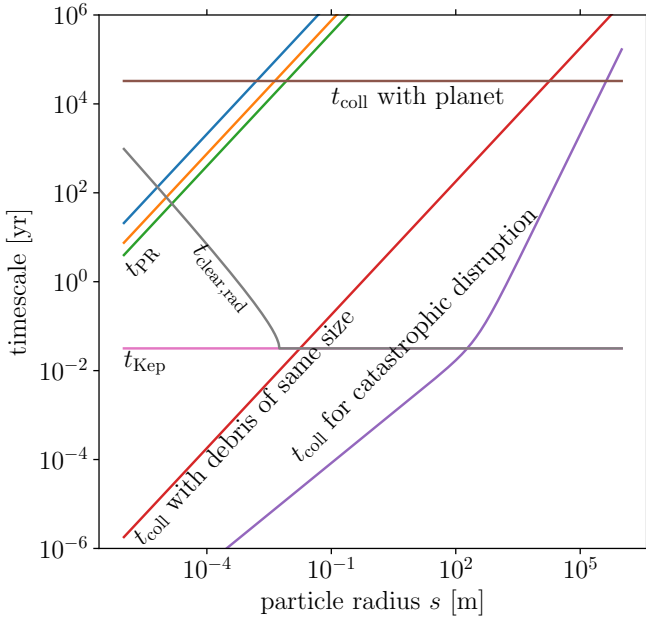


Figure 10. The fate of collision debris produced in a collision at 0.1 au. At this distance, the timescale for re-accretion onto a $1 M_{\oplus}$ planet is almost 10^4 yr (brown line). This is shorter than the lifetime under PR drag for particles ≥ 1 mm in size (diagonal green, orange, blue lines show the time for particle orbits to shrink 10, 20 and 100%). However, these particles will collide and be destroyed by other debris particles on still shorter timescales, less than one orbital timescale for bodies ≤ 1 cm in size (Diagonal red line shows the time to collide with another debris particle if the size distribution is monodisperse; bent purple line shows the time to experience a catastrophic disruption with a smaller debris particle). A collisional cascade would then quickly reduce these particles to the blow-out limit ($\sim 1 \mu\text{m}$), where they are removed from the system by radiation pressure on a dynamical time-scale (horizontal pink line). If a significant number of small particles are generated, however, the disc becomes optically thick. Blow-out grains are only removed if they exist on high-inclination orbits where the optical depth to the star $\tau_{\text{rad}} \leq 1$. The time-scale for this process, $t_{\text{clear,rad}}$ (grey line), is still shorter than the time-scales for re-accretion by the planet and for PR drag to remove the particles.

only one or even zero large ($> 1 M_{\oplus}$) planets, particularly when the initial embryo mass is smaller ($0.05 M_{\oplus}$). This is true so long as collision fragments are swiftly removed from the system and do not reaccrete. As pointed out above, however, there is a potential fine-tuning issue in getting enough single-planet systems in these simulations.

7.2 The fate of the collision debris

We now revisit the fate of the collision debris. Debris is removed from systems by several processes. Small grains ($\leq 1 \mu\text{m}$ for a G-type star) are removed by radiation pressure on a dynamical time-scale, while larger grains experience orbital decay through Poynting–Robertson drag (Burns et al. 1979). They are also reduced to smaller sizes through destructive collisions; the subsequent collisional cascade results in the particles eventually being ground small enough to be removed by radiation pressure. The key question is whether these removal methods occur faster than the parent planets will re-accrete the debris.

The debris will emerge from the collision with a certain size

distribution. In their numerical experiments, Leinhardt & Stewart (2012) found a very steep size distribution with most of the mass in the smallest fragments; in terms of diameter D ,

$$n(D)dD = CD^{-(\beta+1)}dD \quad (7)$$

where β ranges from 2.5 to 5.2 with a median of 3.8 (their Equation 31 and Table 1). Furthermore, as well as larger gravitationally-bound fragments, some ejecta will be in the form of small melt droplets: Benz et al. (2007) found that the size distribution of ejecta peaked at $s \sim 1$ cm in their simulations of collisional stripping of Mercury’s mantle. Here we initially assume a monodisperse population of debris fragments and then consider a more realistic continuous distribution. In general, the more the size distribution is weighted towards smaller particles, the shorter the lifetime of the debris.

Consider a collision at $a = 0.1$ au that creates a monodisperse population of grains with radius s and the combined mass of a body of radius $s_{\text{eq}} = 1000$ km, and that leaves a $1 M_{\oplus}$, $1 R_{\oplus}$ planet at 0.1 au. Assume that the grains have a mean orbital eccentricity of $\langle e \rangle = 0.2$. The time-scale for reaccretion onto the planet, including the effects of gravitational focusing (fairly unimportant at these orbital velocities, increasing the gravitational cross-section by only 35%), is then $\sim 33\,000$ yr. This is shown as the horizontal brown line in Figure 10. For our neglect of debris to be justified, the particles must be removed on shorter timescales.

Stellar radiation causes a slow decay of particle orbits through the Poynting–Robertson effect (“PR drag”), which causes a low-eccentricity orbit to decay into the star in a time

$$t_{\text{PR}} = a^2/4\alpha \quad (8)$$

where

$$\alpha = \frac{3L_{\star}}{16\pi c^2 \rho s}, \quad (9)$$

L_{\star} being the stellar luminosity and ρ the density of a debris particle. For our particles, it suffices to drift a distance of $\sim a\langle e \rangle$ to prevent reaccretion, leading to a slightly shorter lifetime (diagonal green, orange and blue lines in Figure 10). This is shorter than the reaccretion timescale for mm- to cm-sized particles, and these particles will be removed without significant re-accretion onto the planet. Hence, ignoring collisions between debris fragments, recondensed vapour droplets are lost to PR drag before re-accretion.

However, owing to the large density of particles, the lifetimes of particles of all sizes are in fact also limited by mutual collisions. Considering a monodisperse size distribution, in which every collision is with an equal-mass object and is destructive, the particles have a collision lifetime of

$$t_{\text{coll}} = \frac{t_{\text{Kep}}}{\pi \tau_{\text{eff}}}, \quad (10)$$

where τ_{eff} is the effective face-on optical depth of the annulus of fragments. t_{coll} is shown as the diagonal red line in Figure 10. This is in fact less than the orbital timescale for grains ≤ 1 cm in size, and is less than the timescale for re-accretion onto the planet for all but the largest fragments of $s \geq 10$ km: the surface area of the fragments is always large, and the boost to the planet’s gravitational cross-section through gravitational focusing is modest because of the high orbital velocities. Thus, particles will grind down to the blow-out size and be removed by radiation pressure, just as in typical debris discs (e.g., Wyatt 2005).

Considering a more realistic size distribution can shorten the collision lifetimes among the debris particles significantly. The reason is that a catastrophic disruption of a large fragment can be

induced by a significantly smaller impactor. Assuming for simplicity a bimodal size distribution with equal mass in particles of size s and the smallest particles sufficient to disrupt them yields a lifetime for the larger particles given by the purple line in Figure 10. The kink at ~ 100 m is caused by the change from the gravity-dominated to the strength-dominated regime. These timescales are now smaller than the timescale for re-accretion onto the planet, or comparable to in the case of the largest debris fragments (a few hundred km). However, recall that [Leinhardt & Stewart \(2012\)](#) found that in most cases the fragment distribution was bottom-heavy. Hence, most debris will be ground down to the blow-out size before re-accretion onto the planet.

Finally, the large mass of the debris cloud does however introduce a complication: if most of the grains are $\lesssim 1$ cm in size, the disc becomes optically thick and radiation pressure will be inefficient as an agent of removal. In this case, only grains on high-inclination orbits that can escape the disc mid-plane to less dense high- z regions, where the radial optical depth $\tau_{\text{rad}} \lesssim 1$, will be removed. If we assign the grains a Rayleigh distribution of inclinations with parameter σ_I (in radians), then the optically thin surface is at

$$z_{\text{thin}} = \sqrt{-2a^2\sigma_I \log [2^{3/2}\pi^{1/2}\sigma_I(a/s)^2/N_{\text{part}}]}, \quad (11)$$

where N_{part} is the number of particles. There is then a fraction

$$f_{\text{thin}} = 2\text{sf}(z_{\text{thin}}/a\sigma_I) \quad (12)$$

of grains in the region with $\tau_{\text{rad}} \lesssim 1$, where $\text{sf}(x)$ is the Gaussian survival function. These are removed on a dynamical time-scale, after which the next surface layer of grains becomes exposed; the erosion therefore takes place on a timescale

$$t_{\text{clear}} = t_{\text{Kep}}/f_{\text{thin}}. \quad (13)$$

For our parameters, the removal timescale is equal to the orbital timescale for the optically thin discs with $s \gtrsim 1$ cm, and rises to ~ 1000 yr if all of the mass is in small grains. This is still considerably lower than the timescale for re-accretion onto the planet, justifying our neglect of the debris. This timescale is plotted in Figure 10 as the grey line.

We repeated these calculations for an orbital radius of 1 au. Here the size where the mutual collision timescale exceeds that for re-accretion onto the planet falls to 100 km. We also repeated the calculations at 0.1 au but with half the e and i of the fragments. This reduced the timescale to collide with the planet, and slightly increased the lifetime of debris particles to mutual collisions, but the mutual collision lifetime remained shorter than the re-accretion time for bodies under a few hundred km.

7.3 Conclusions

We have implemented a collision algorithm into MERCURY that improves on the standard algorithm that collisions between planets always result in perfect merging. We tested the effects of this on the outcome of N -body integrations of unstable multi-planet systems close to the star, systems destabilised by outer planets, and *in-situ* formation of rocky super-Earths. In general, the effects of adopting the improved collision algorithm are greater when the ratio of the collision velocity to the escape velocity rises, such as when planetary orbits are smaller, eccentricity excitation is stronger, or planets are of lower mass. Specifically, we find the following:

- Collisions between transiting planets at ~ 0.1 au are frequently erosive. Perfect mergers only account for 40% of collisions in our

fiducial case of an unstable system of five super-Earths where the innermost is located at 0.1 au (Figure 4).

- The fraction of mass lost to collisional debris in these systems is $\sim 10\%$ of the initial planetary mass. Hence, the mass distribution and system multiplicity after instability is not strongly affected compared to running simulations with only perfect merging (Figure 5). However, the collision algorithm does have some effect on the final separations of planets: surviving two-planet systems are more widely spaced with the improved collision algorithm than when run with the standard algorithm (Figure 7). Furthermore, we can expect the distribution of planetary radii to be more strongly affected due to the strong dependence of planet radius on envelope mass for planets with small hydrogen/helium envelopes.

- The fraction of collisions resulting in perfect mergers rises as planets' semimajor axis is increased and decreases as planets' mass is decreased. It is fairly insensitive to the initial separation of planets (in mutual Hill radii). There is a small effect when starting from very flat configurations $i \sim 0.1^\circ$ (Figures 4, 6).

- Transiting systems destabilised by eccentric outer bodies (giant planets experiencing Kozai cycles or planet–planet scattering) experience a smaller fraction of perfect mergers (20 – 30%), and the effects of a realistic collision prescription are more significant in such systems (Figure 8).

- Smaller planets, or planetary embryos, suffer more from erosive collisions. This affects the outcome of planet formation *in situ* from smaller embryos. If collisional debris is rapidly removed from the system (for example, by radiation forces) then *in-situ* formation forms fewer, more widely-spaced planets with the improved collision algorithm than when assuming that all collisions result in perfect merging (Figure 9). This may provide a contribution towards explaining the *Kepler* dichotomy, at least for smaller, rocky, planets. However, if debris is not quickly removed, then reaccretion will lead to higher-multiplicity systems similar to those formed if collisions always result in perfect mergers.

ACKNOWLEDGEMENTS

The authors are supported by the project grant 2014.0017 ‘‘IMPACT’’ from the Knut and Alice Wallenberg Foundation. A.J. was supported by the European Research Council under ERC Consolidator Grant agreement 724687-PLANETESYS, the Swedish Research Council (grant 2014-5775) and the Knut and Alice Wallenberg Foundation (grants 2012.0150, 2014.0017, and 2014.0048). The simulations were performed on resources provided by the Swedish National Infrastructure for Computing (SNIC) at Lunarc. This research has made use of the Exoplanet Orbit Database and the Exoplanet Data Explorer at exoplanets.org. We thank the referee, John Chambers, for a careful and insightful referee report.

REFERENCES

- Ballard S., Johnson J. A., 2016, *ApJ*, **816**, 66
 Batygin K., Morbidelli A., Holman M. J., 2015, *ApJ*, **799**, 120
 Benz W., Asphaug E., 1999, *Icarus*, **142**, 5
 Benz W., Slattery W. L., Cameron A. G. W., 1988, *Icarus*, **74**, 516
 Benz W., Anic A., Horner J., Whitby J. A., 2007, *Space Sci. Rev.*, **132**, 189
 Burns J. A., Lamy P. L., Soter S., 1979, *Icarus*, **40**, 1
 Carrera D., Davies M. B., Johansen A., 2016, *MNRAS*, **463**, 3226
 Carter P. J., Leinhardt Z. M., Elliott T., Walter M. J., Stewart S. T., 2015, *ApJ*, **813**, 72
 Chambers J. E., 1999, *MNRAS*, **304**, 793

- Chambers J. E., 2013, *Icarus*, 224, 43
- Chambers J. E., 2016, *ApJ*, 825, 63
- Chambers J. E., Wetherill G. W., Boss A. P., 1996, *Icarus*, 119, 261
- Chatterjee S., Ford E. B., 2015, *ApJ*, 803, 33
- Chatterjee S., Tan J. C., 2014, *ApJ*, 780, 53
- Delisle J.-B., Laskar J., 2014, *A&A*, 570, L7
- Duchêne G., Kraus A., 2013, *ARA&A*, 51, 269
- Faber P., Quillen A. C., 2007, *MNRAS*, 382, 1823
- Fabrycky D. C., et al., 2014, *ApJ*, 790, 146
- Fang J., Margot J.-L., 2012, *ApJ*, 761, 92
- Fulton B. J., et al., 2017, preprint, ([arXiv:1703.10375](https://arxiv.org/abs/1703.10375))
- Genda H., Kokubo E., Ida S., 2012, *ApJ*, 744, 137
- Genda H., Fujita T., Kobayashi H., Tanaka H., Abe Y., 2015, *Icarus*, 262, 58
- Han E., Wang S. X., Wright J. T., Feng Y. K., Zhao M., Fakhouri O., Brown J. I., Hancock C., 2014, *PASP*, 126, 827
- Hansen B. M. S., Murray N., 2012, *ApJ*, 751, 158
- Hansen B. M. S., Murray N., 2013, *ApJ*, 775, 53
- Huang C. X., Petrovich C., Deibert E., 2017, *AJ*, 153, 210
- Izidoro A., Ogihara M., Raymond S. N., Morbidelli A., Pierens A., Bitsch B., Cossou C., Hersant F., 2017, preprint, ([arXiv:1703.03634](https://arxiv.org/abs/1703.03634))
- Jackson A. P., Wyatt M. C., 2012, *MNRAS*, 425, 657
- Johansen A., Davies M. B., Church R. P., Holmelin V., 2012, *ApJ*, 758, 39
- Laskar J., Gastineau M., 2009, *Nature*, 459, 817
- Leinhardt Z. M., Stewart S. T., 2012, *ApJ*, 745, 79
- Leinhardt Z. M., Dobinson J., Carter P. J., Lines S., 2015, *ApJ*, 806, 23
- Lissauer J. J., et al., 2011, *ApJS*, 197, 8
- Lissauer J. J., et al., 2014, *ApJ*, 784, 44
- Liu S.-F., Agnor C. B., Lin D. N. C., Li S.-L., 2015, *MNRAS*, 446, 1685
- Marcus R. A., Stewart S. T., Sasselov D., Hernquist L., 2009, *ApJ*, 700, L118
- Matsumoto Y., Kokubo E., 2017, *AJ*, 154, 27
- Melis C., Zuckerman B., Rhee J. H., Song I., 2010, *ApJ*, 717, L57
- Moriarty J., Ballard S., 2016, *ApJ*, 832, 34
- Moriarty J., Fischer D., 2015, *ApJ*, 809, 94
- Movshovitz N., Nimmo F., Korycansky D. G., Asphaug E., Owen J. M., 2016, *Icarus*, 275, 85
- Mustill A. J., Veras D., Villaver E., 2014, *MNRAS*, 437, 1404
- Mustill A. J., Davies M. B., Johansen A., 2015, *ApJ*, 808, 14
- Mustill A. J., Davies M. B., Johansen A., 2017, *MNRAS*, 468, 3000
- Ogihara M., Morbidelli A., Guillot T., 2015, *A&A*, 578, A36
- Pu B., Wu Y., 2015, *ApJ*, 807, 44
- Quillen A. C., 2011, *MNRAS*, 418, 1043
- Quillen A. C., Bodman E., Moore A., 2013, *MNRAS*, 435, 2256
- Quintana E. V., Barclay T., Borucki W. J., Rowe J. F., Chambers J. E., 2016, *ApJ*, 821, 126
- Reinhardt C., Stadel J., 2017, *MNRAS*, 467, 4252
- Schlichting H. E., 2014, *ApJ*, 795, L15
- Smith A. W., Lissauer J. J., 2009, *Icarus*, 201, 381
- Song I., Zuckerman B., Weinberger A. J., Becklin E. E., 2005, *Nature*, 436, 363
- Spalding C., Batygin K., 2016, *ApJ*, 830, 5
- Theissen C. A., West A. A., 2017, *AJ*, 153, 165
- Tremaine S., Dong S., 2012, *AJ*, 143, 94
- Valencia D., Sasselov D. D., O'Connell R. J., 2007, *ApJ*, 665, 1413
- Volk K., Gladman B., 2015, *ApJ*, 806, L26
- Wallace J., Tremaine S., Chambers J., 2017, *AJ*, 154
- Weiss L. M., Marcy G. W., 2014, *ApJL*, 783, L6
- Weiss L. M., et al., 2017, preprint, ([arXiv:1706.06204](https://arxiv.org/abs/1706.06204))
- Wyatt M. C., 2005, *A&A*, 433, 1007
- Wyatt M. C., Smith R., Greaves J. S., Beichman C. A., Bryden G., Lisse C. M., 2007, *ApJ*, 658, 569
- Zhu W., Petrovich C., Wu Y., Dong S., Xie J., 2018, preprint, ([arXiv:1802.09526](https://arxiv.org/abs/1802.09526))

This paper has been typeset from a $\text{\TeX}/\text{\LaTeX}$ file prepared by the author.